

NUMERICAL ANALYSIS OF TARGET ENUMERATION VIA EULER CHARACTERISTIC INTEGRALS: 2 DIMENSIONAL DISK SUPPORTS

SAM KRUPA

*With tremendous help from Professor Michael Robinson and Professor Robert Ghrist.
Funding gratefully acknowledged from DARPA & the ONR.*

ABSTRACT. In this paper, we look at the types of errors that are introduced when using the Euler characteristic integral approach to count the number of targets in a discrete sensor field. In contrast to other theoretical analyses, this paper examines discrete sensor fields rather than continuous ones. The probabilities of first and second order errors are worked out combinatorially, and a general formula is found which is discovered to be proportional to much higher order errors. Asymptotic results are also derived. Thus, this work gives us the bias of the Euler characteristic integral as a point estimator for the number of targets in a sensor field, and a general understanding of how the Euler characteristic integral fails, or more often succeeds.

1. INTRODUCTION

Imagine a planar sensor field in a region $\Omega \subset \mathbb{R}^2$ that is infinitely dense, with infinitesimally small sensors. Each point $x \in \Omega$ has a sensor which records simply the number of objects directly over it. Throw many objects of any shape onto this field, and as long as their 2-dimensional projections have identical Euler characteristics $\neq 0$, using the work of Robert Ghrist and Yuliy Baryshnikov ([1], [2]), the number of objects (or *targets*) can be exactly determined using nothing but the sensor field data recorded, which is the location of each sensor and how many objects overhead it detects.

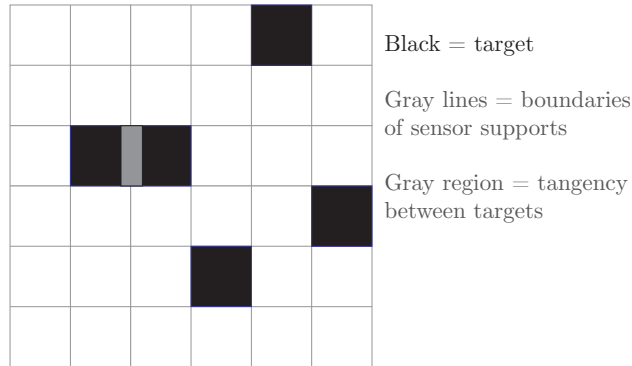


FIGURE 1. A sensor grid. The union of each sensor's 1×1 area makes up the entire field. When two targets are almost tangent with no overlap but no sensor in between, they become impossible to differentiate. The tangency above (highlighted in gray) causes the two targets to appear as one.

Now discretize the sensor field, take away its infinite sensor density, and errors will be introduced into the above solution of this target enumeration problem. The most obvious error occurs when two targets do not overlap, but there is no sensor in between them to differentiate them from one another, so they appear instead to be one large target (see figure 1) – no algorithm could detect two targets here unless information on the targets’ shapes is given.

This paper is a numerical analysis of the target enumeration via Euler characteristic integral technique given by Ghrist and Baryshnikov. It proceeds by analyzing the causes of the most common first order (section 2.4) and second order errors (2.5) in target enumeration when the sensor field is discretized, then combinatorial arguments are given for the probabilities of these different errors under the assumption that the targets’ 2-dimensional projections are disk shaped and targets fall onto the sensor field under a uniform distribution. With these probabilities calculated, the errors can be added back and the correct number of targets can be better approximated (2.6). We then derive an asymptotic result for how the Euler characteristic integral behaves for large numbers of targets (3).

1.1. A survey of the field. Tomorrow’s man will step into a world that is inundated with what we call today “sensors.” Fields of sensors will count him as he steps onto the street, as he drives his hover car, and when he steps onto the battlefield. Tiny sensors will precisely read his DNA. Other sensors will tirelessly count the pesticide molecules on his vegetables. Sensors of all sorts will appear to read his mind, returning data to him just when he needs it. These same sensors will feed smart algorithms working to improve traffic flow, crop development, and battlefield awareness [7]. But before this world can exist for our everyman to experience, much work needs to be done.

The study of sensor networks is nascent, and the fundamentals are still being developed. There are many different problems which need to be solved. There are research groups working on networking, communication, and signal processing algorithms to connect individual sensors into working, collaborative sensor fields using minimal computing resources and energy ([4], [8], [9], [15], amongst many others). Another team is working on monitoring and making sense of data coming off real world sensor fields with broken and malfunctioning sensors [19]. And finally, complete mathematical theories for target enumeration and tracking via fields of sensors are just starting to be developed.

The problem of interest here is *target enumeration*: given the return of a sensor field, how best to fuse the data from the individual sensors so as to count the total number of unique targets being picked up by the sensor field.

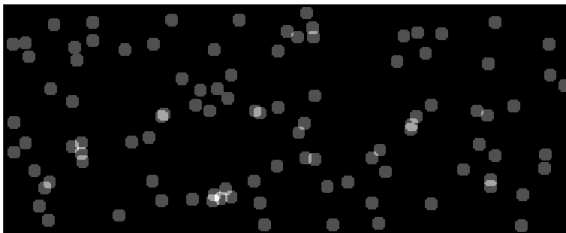


FIGURE 2. A visualization of the return of a typical discretized sensor grid, as will be studied throughout this paper. This sensor grid is 200×500 , and 100 targets of radius 6 have been placed over it. A sensor with as many or more targets over it then all other sensors is painted white, a sensor with no target over it is painted black, and all other sensors are painted on a sliding scale between white and black.

Much of the current work in target enumeration or the closely related field of target tracking, such as [9], [11], and [12], assumes targets that in one way or another are each easily detected and differentiated from one other. However, other teams have worked on solving the *complete* target counting and tracking problem where targets are less easily differentiated from one other and from their environment.

One team has analyzed target enumeration with binary sensors, which each return a result from $\{0, 1\}$ [18]. They found that for any fixed time, not enough information is contained in a binary sensor field to return an accurate estimate of the number of targets. But by looking at time series data through a particle filter, both target counts and target trajectories can be nicely approximated under the weak assumption of relatively small changes in target velocity vector moment to moment. Even using real world sensors, the results are impressive. However, the techniques have so far only been developed in one space dimension and no theoretical efficacy analysis has been done.

Given a sensor field where each sensor picks up a voltage inversely proportional to the distance from each target, additive over each target, one team [8] has worked on counting the number of targets picked up by this field by counting the number of relative maxima in the returned voltages. However, their methods fail when targets are insufficiently separated or are in other complex arrangements. The authors try to reduce errors by intelligently turning on and off sensors and carefully tracking the effects of noise. They place approximate bounds on the expected errors in their methods, but again no close analysis of how errors accumulate under their algorithms has been performed.

The most complete, but also the most theoretical, work to date on a solution to the problem of target enumeration has been done by Y. Baryshnikov and R. Ghrist using the topological technique of the integral with respect to the Euler characteristic ([1], [2]). Here the theory has been substantially worked out and, at least in the case of infinitely dense continuous sensor fields, is able to accurately count targets which are in very complex configurations using sensors which return only local target counts. Further, the expected Euler characteristic integral of a Gaussian random field has been worked out, which allows for unbiased target enumeration from noisy sensor fields [3]. However, until now nothing more than conjecture has existed concerning numerical analysis of the Euler characteristic integral when our sensor field is discretized.

We begin here with a preliminary numerical analysis of the Euler characteristic integral as a tool for target enumeration, picking up where Baryshnikov and Ghrist left off. We make exacting and precise assumptions, and derive expectations for the number of miscounted targets in a discrete sensor field when the enumeration via Euler characteristic integral theory is applied. We gain an understanding into how different types of discretization errors occur, and the result is the only technique that we know of to unbiasedly, to an approximation, count the number of targets in a discrete sensor field returning only local target counts at each sensor.

1.2. Background. Before we can present the main result we use in topological target enumeration, we need a few definitions. The sensors in this paper are thought of as 2-dimensional squares and as detecting all targets directly above them, and the targets can be thought of as being not point particles but 2-d laminae. A sensor field, discrete or continuous, has a corresponding *height function* $h(x) \in \mathbb{Z}$ which at each point x in the sensor field $\Omega \subset \mathbb{R}^2$ returns the number of targets the sensor at x is detecting. Note that even when the sensor field is discrete, its height function can still be thought of as coming from a continuous sensor field. We give the following definition [1]:

Excursion sets: For functions $h : X \rightarrow \mathbb{Z}$, the set $\{h = s\}$ is the *level set* $\{x \in X : h(x) = s\}$, and the set $\{h > s\}$ is the *upper excursion set* $\{x \in X : h(x) > s\}$. Lower excursion sets are likewise defined.

In the continuous case, the formula for the number of targets (with Euler characteristic = 1) in a given sensor field is the duality formula *Theorem 4.3* in Ghrist and Baryshnikov:

Theorem 1.1 ([1, Theorem 4.3]). *For $h : \mathbb{R}^2 \rightarrow \mathbb{N}$ constructible and upper semicontinuous,*

$$\int_{\mathbb{R}^2} h d\chi = \sum_{s=0}^{\infty} (\beta_0\{h > s\} - \beta_0\{h \leq s\} + 1),$$

where β_0 denotes the zeroth Betti number, or equivalently, the number of connected components of the set.

Constructible functions are “tame” and integer-valued on a topological space (for a quick introduction, see [2]).

While not thoroughly tested in their article [1], Ghrist and Baryshnikov expect (1.1) to be the most numerically stable of all equivalent formulae.

2. NUMERICAL ANALYSIS

In this paper, we study ideal discrete sensor fields, which are made up of a finite number of sensors, all of which are assumed to be performing their function without error. Here, the object of our study is discrete sensor fields which are made up of collections of square sensors of area 1×1 which detect perfectly the number of targets above them. These sensors can also be thought of as point particles with square sensing regions. The sensors are then arranged in regular grids with no overlap or space among them.

We define the height function $h(x)$ for the sensor field such that for x not along the boundary of any sensor support, $h(x)$ returns the total number of targets above that sensor whose sensing region contains x . In our construction of an ideal discrete sensor field, there is no sensing region along the boundaries of the sensor supports, and any target without width that lies entirely along the boundaries of sensor supports will not be picked up by our sensor field. Then for x along the boundary of a sensor support, we define $h(x)$ such that its value agrees with the value returned by the sensor underneath or to the left of x .

This discretization of the sensor field changes the basic behavior of the Euler characteristic integral in two important ways, which we now note below.

2.1. Finite field discretization errors. When using Theorem 1.1 to evaluate the Euler characteristic integral over a *bounded* (and connected) region Ω , we need to be careful. Suppose, for instance, the height function $h = 10$ throughout Ω , so that h never vanishes along $\partial\Omega$. Then the calculated value of the integral using Theorem 1.1 is 20. This differs from the correct value of 10 by a factor of 2 (see figure 3a). To correct this error, we can zero-pad h by constructing a function g such that,

$$g(x) = \begin{cases} h(x) & \text{if } x \in \Omega \\ 0 & \text{if } x \notin \Omega \end{cases}$$

and then integrating g over \mathbb{R}^2 instead of h over Ω . For the rest of this paper, this correction is always assumed to be made when working with finite, discrete sensor fields.

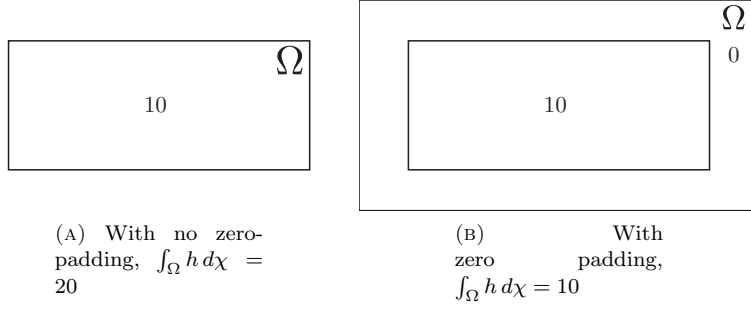
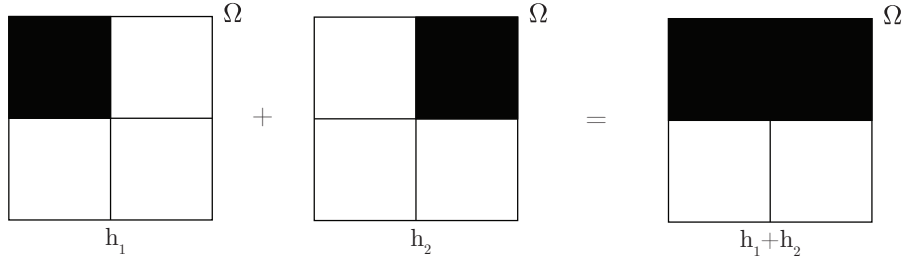


FIGURE 3. The Euler characteristic integrals of the returns of these two sensor fields show the effect on the integral caused by zero-padding the sensor field data.

2.2. Linearity of the discrete Euler characteristic integral. Under discrete sensor fields, linearity of the Euler characteristic integral (which is true for continuous sensor fields) does not hold. Take for instance two height functions (h_1 and h_2) each generated by sensor fields of four sensors arranged in a square grid, where one small target is placed on each field. Then, with black indicating function value of 1 and white indicating 0,



Note that $\int_{\Omega} h_1 d\chi = 1$ and $\int_{\Omega} h_2 d\chi = 1$, but $\int_{\Omega} (h_1 + h_2) d\chi = 1 \neq 1 + 1 = 2$. Thus, over discrete sensor fields the Euler characteristic integral is not a linear operator.

However, one particular instance of linearity still holds for discrete sensor fields.

Lemma 2.1. *For any positive integer n ,*

$$(1) \quad \int_{\Omega} \sum_{i=1}^n h d\chi = n \int_{\Omega} h d\chi$$

Proof. This is a result known [5] to hold over continuous sensor fields, but as seen above that does not necessarily mean the result holds over discrete sensor fields. Thus we argue as follows to show the result continues to hold over discrete sensor fields.

Note,

$$(2) \quad \beta_0\{nh > nk + i\} = \beta_0\{h > k\}$$

$$(3) \quad \beta_0\{nh \leq nk + i\} = \beta_0\{h \leq k\}$$

for all $i = 0, 1, 2, \dots, n-1$ and for all $k = 0, 1, 2, 3, \dots$. Then,

$$\begin{aligned} \int_{\Omega} \sum_{i=1}^n h d\chi &= \sum_{s=0}^{\infty} (\beta_0\{nh > s\} - \beta_0\{nh \leq s\} + 1) \\ &= \sum_{i=0}^{n-1} \sum_{k=0}^{\infty} (\beta_0\{nh > nk + i\} - \beta_0\{nh \leq nk + i\} + 1) \end{aligned}$$

and then by (2) and (3),

$$\begin{aligned} &= \sum_{i=0}^{n-1} \sum_{k=0}^{\infty} (\beta_0\{h > k\} - \beta_0\{h \leq k\} + 1) \\ &= n \sum_{k=0}^{\infty} (\beta_0\{h > k\} - \beta_0\{h \leq k\} + 1) \\ &= n \int_{\Omega} h d\chi \end{aligned}$$

which proves the statement. \square

2.3. Analysis of target enumeration. The numerical properties of Theorem 1.1, as a point estimator for target enumeration in discrete sensor fields, depend entirely on the magnitude, shape, and distribution of the targets, as well as the setup of the sensor field. For example, the smaller the targets, the less likely a tangency is to occur for a given sensor field size. We first consider tiny targets, smaller than the individual sensor size. Given a large sensor field, the probability that two of these tiny targets will appear tangent and cause an error is much smaller than when large disks are being placed on a sensor field of the same size, as each large disk has a large perimeter to which another target can come in contact. Noncircular objects have their own sets of problems. Imagine, for instance, a star-shaped target and a disk-shaped target of similar magnitude: the disk has far less perimeter, and cannot interact with other disks in the way a star could interact with other stars. Moreover, the more uniformly spread out our targets, the less likely an error is to occur, in contrast to all the targets being concentrated in a single part of our sensor region Ω . So, for our analysis we will impose a few constraints:

- (1) There are n targets, each of which are disks of the *same* integer radius $r \leq 7$.
- (2) Targets are discretely placed with integer center coordinates.
- (3) The equation for the discrete disks which will approximate our targets is $x^2 + y^2 < r^2$ and not $x^2 + y^2 \leq r^2$ as the latter formulation introduces extraneous features into the discrete disks (see figure 4).
- (4) Sensor field region is rectangular, $l \times w$, and the sensor field is made up of a regular grid of $l \cdot w$ sensors, each having a size of 1×1 . The union of the sensors gives us the complete sensor field.
- (5) Targets' centers are uniformly distributed over our region.
- (6) To prevent edge effects, targets' centers are kept a minimum of r units away from edge.

For a detailed analysis of discrete integer radius circles with integer centers (known as *Freeman digitizations*) see [13].

We proceed with calculating the expectation of $\int_{\mathbb{R}^2} h d\chi$ when the integral is calculated using Theorem 1.1, and the assumptions are as above. First, note

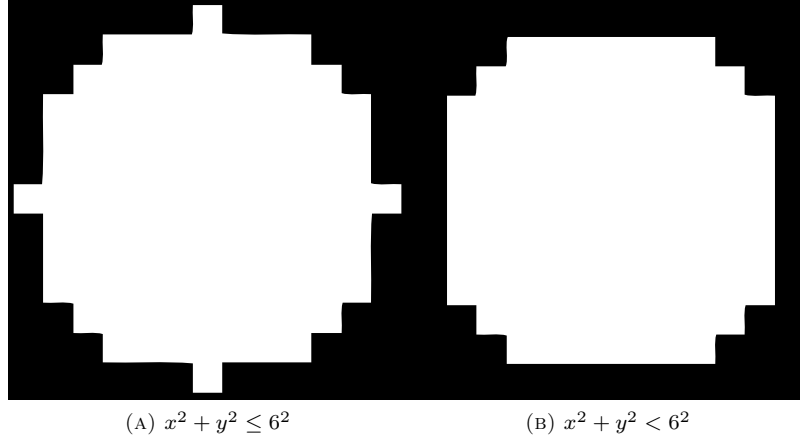


FIGURE 4. A comparison of two different formulae for discrete disks.

$$(4) \quad \mathbb{E} \left(\int_{\mathbb{R}^2} h d\chi \right) = n - \mathbb{E}(\text{number of errors})$$

where *errors* are the number of miscounted targets, the deviation from the true value of n targets.

2.4. First order approximation. A first order approximation would be to count the number of tangencies amongst the targets, and take this as an estimate of the error. Let's do that.

$$\begin{aligned}
 \mathbb{E}(\# \text{ of errors}) &\approx \mathbb{E}(\# \text{ of tangencies}) \\
 &= \mathbb{E} \left(\sum_{i=1}^n \# \text{ tangencies on disk } i \right) \\
 &= \sum_{i=1}^n \mathbb{E}(\# \text{ tangencies on disk } i) \\
 &= \sum_{i=1}^n (n-1) \cdot \Pr(\text{one of the other } n-1 \text{ disks comes tangent to disk } i) \\
 &= n \cdot (n-1) \cdot \Pr(\text{one of the other } n-1 \text{ disks comes tangent to disk } i)
 \end{aligned}$$

Then ignoring edge effects for a moment,

$$(5) \quad = n \cdot (n-1) \cdot \frac{b}{(x-2r)(y-2r)}$$

This is by linearity of expectation, the disks' centers being independently and identically distributed uniform random variables, and the fact that only an area of $(x-2r)(y-2r)$ is available for the centers to be placed. Here $b = 88$, for example, in the case of radius = 6 disks. There are 88 points

around one disk where the center of another identical disk can be such as to cause a tangency – as shown by the white ring around the radius = 6 discrete disk in figure 5.

It is important to note that due to edge effects, even as an expected value of the number of tangencies and not errors, the above formula is an approximation. The average radius = 6 disk picked up by our sensor field doesn't have quite 88 spots around it where another disk can be placed to cause tangency; disks closer to the edge cannot have another disk placed to one side of them (see figure 6). So (5) becomes a better and better approximation to the number of tangencies as $x, y \rightarrow \infty$. The magnitude of this error is most notable when placing radius r disks down on a $2r \times 2r$ sensor field without boundary effects: no matter how many disks are put down, as there is only one location where the target can fall, no tangencies will occur.

We can correct for edge effects thusly. Assume our region is larger than $4r \times 4r$. Put a disk at each of the $2 \cdot \text{radius}$ points closest to the boundary, and for each disk calculate at how many points in our region another disk could be placed to cause a tangency. Over the $2 \cdot \text{radius}$ boundary locations, calculate the average number of tangency points for a disk centered at each location. Then we can calculate a weighted average representing the number of tangency points the average disk in our region is expected to have, which is a corrected value for our number of tangency points and is lower than the value calculated neglecting edge effects.

Let α = average number of tangency points in boundary region and β = number of tangency points of disk neglecting edge effects such that, in a region Ω of dimension $l \times w$,

$$\text{corrected (average) \# tangency points for a discrete disk (of radius } r) \text{ in } \Omega = \frac{(l \cdot w - (w - 4 \cdot r) \cdot (l - 4 \cdot r)) \cdot \alpha + (w - 4 \cdot r) \cdot (l - 4 \cdot r) \cdot \beta}{\text{total area of } \Omega}$$

Experimental results (table 2) suggest equation (5) holds as an approximation to the number of errors as long as targets (disks in this case) are not too densely packed allowing for many higher-order errors to occur; but this approximation still becomes poor very fast.

So we need to find the next set of second order errors.

2.5. Second order approximation.

Theorem 2.2 (Second order error approximation formula). *For simplicity assuming a radius of 6, letting $88_{\text{corrected}}$ denote the number of tangency points of a radius 6 disk corrected for edge effects*

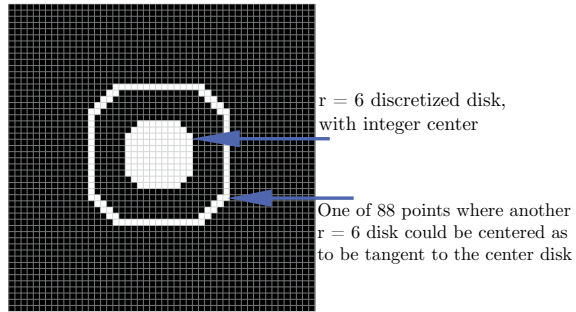


FIGURE 5. The white ring contains 88 points where a disk of radius 6's center can be placed, such as to cause a tangency with the center disk of radius 6.

and $A = (x - 2r)(y - 2r)$, a second-order estimate of $n - E(\int_{\mathbb{R}^2} h d\chi)$ is given by

$$(6) \quad E_n \approx \frac{88_{corrected}}{c^2} \left(\left(1 - \frac{c}{A}\right)^n \cdot A - A + nc \right)$$

where c is a proportionality constant and when the conditions assumed in the beginning of section 2 are met.

As a first step towards proving (6), let's calculate the Euler characteristic integral of a few different sensor fields to get a feel for how errors accumulate. See figure 7.

In 7a, there is one tangency and one error. In 7b, however, there are two tangencies but still only one error. The third disk put down over the second *discriminates* itself by creating a new *2-segment* in the level sets (i.e. there is now an additional connected component in the $\{h = 2\}$ level set). This is the key insight in our derivation of (6): going from 7a to 7b, the total number of errors does not increase. Appropriate generalizations also apply. We can shift the 3rd disk (see 7c), and as long as it still discriminates itself against the 2nd disk the 3rd disk's tangency with the first disk does not lead to an error. Note similar phenomena in 7d and 7e.

On our way to proving (6), the above first suggests the following lemma.

Lemma 2.3. *Given a discrete sensor field with n disk-shaped targets of radius 6 discretely and uniformly placed over it as assumed in the beginning of section 2,*

$$(7) \quad E_n(\# \text{ of errors}) \approx E_{n-1} + \frac{(n-1)88_{corrected}}{A} - \frac{c \cdot E_{n-1}}{A}$$

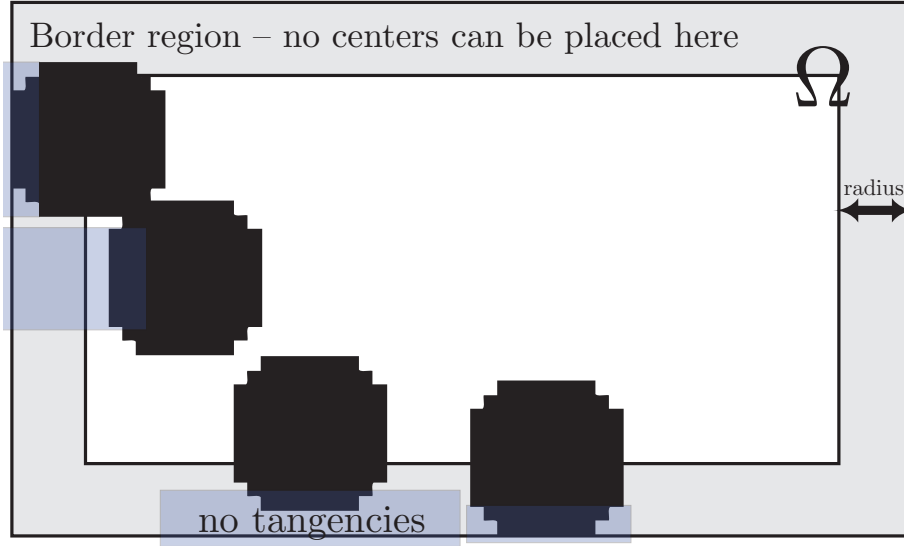


FIGURE 6. Any radius = 6 disk less than $2 \cdot \text{radius}$ from the edge of the region Ω has less than 88 points around it which can cause a tangency if another disk is centered at one of them. This on average reduces the constant b in the tangency calculation formula.

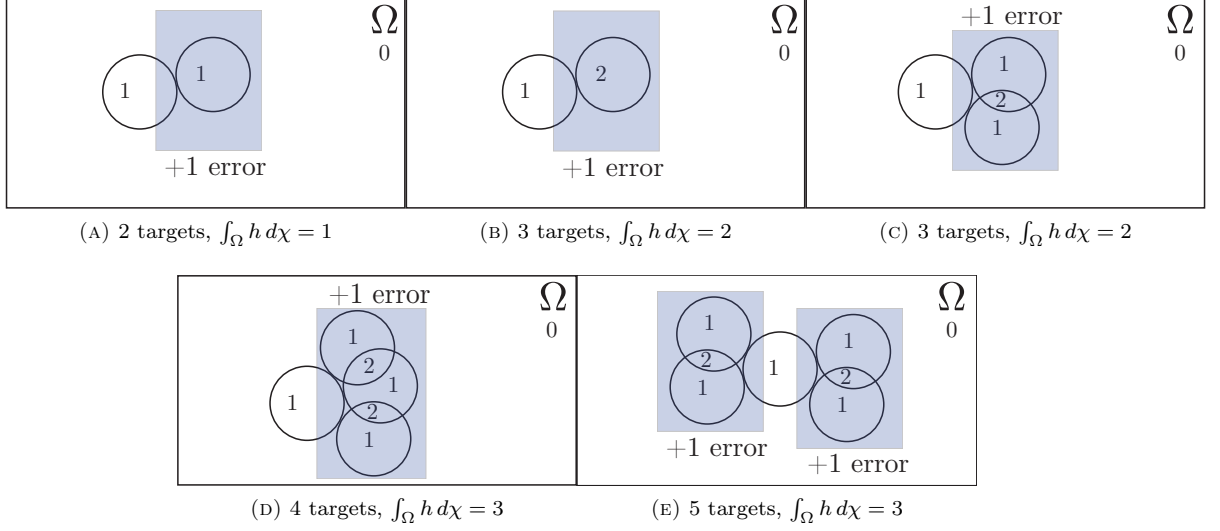


FIGURE 7. Above are the height functions returned by 5 different sensor fields, and their Euler characteristic integrals.

Proof. Put down the first target,

$$E_1(\# \text{ of errors}) = 0$$

Put down the 2nd target, and there is one target it can come tangent to,

$$E_2(\# \text{ of errors}) = \frac{88_{corrected}}{A}$$

Put down the 3rd target and there are two targets it can come tangent to in such a way as to create an error, but some some positions will also cause the 3rd target to be discriminated. The number of such positions is related to the number of tangencies already present, the expected number of which we already calculated above. So,

$$E_3(\# \text{ of errors}) \approx \frac{88_{corrected}}{A} + \frac{2 \cdot 88_{corrected}}{A} - c \cdot \frac{(\text{previous number of tangencies})}{A},$$

by the uniform distribution of target centers, and where c is a proportionality constant. We are subtracting off from the probability that the 3rd target creates a tangency, the probability that the 3rd target does not create an error, for as noted going from 7a to 7b the number of errors does not increase.

$$\begin{aligned} E_3(\# \text{ of errors}) &\approx \frac{88_{corrected}}{A} + \frac{2 \cdot 88_{corrected}}{A} - c \left(\frac{88_{corrected}}{A^2} \right) \\ &= \frac{3 \cdot 88_{corrected}}{A} - c \left(\frac{88_{corrected}}{A^2} \right) \end{aligned}$$

For radius = 6, and given two tangent disks, there are on average (for the 88 possible setups, with a “center disk” held fixed) 21.455 points where a case such as either 7b or 7c can occur, so we take $c = 21.455$ for second-order errors (see figure 8). The value 21.455 is an exact value calculated by an exhaustive search of all possible points for a third disk, averaged over all 88 possible setups.

Next, put down the 4th target. Note that in our second-order-error world, E_3 equals the number of 7a, 7b, or 7c type situations that are expected to occur. We take each of these situations represented by E_3 to have on average $c = 21.455$ points around them where another disk can be centered such as to not cause an error, while still causing a tangency (see figure 8). So, as part of calculating the expected number of errors, when calculating the number of tangencies adding a 4th target is expected to create, we subtract off the probability of one of these tangencies being created by a target being centered at one of the $c \cdot E_3$ “good points.” So,

$$\begin{aligned} E_4(\# \text{ of errors}) &\approx E_3 + \frac{3 \cdot 88_{\text{corrected}}}{A} - c \left(\frac{E_3}{A} \right) \\ &= \frac{6 \cdot 88_{\text{corrected}}}{A} - \frac{4c \cdot 88_{\text{corrected}}}{A^2} + \frac{c^2 88_{\text{corrected}}}{A^3} \end{aligned}$$

What we are studying here is the case where a “center” disk is held in a fixed position, has a height function of 1, and there is a 2nd disk tangent to this center disk. A 3rd disk tangent to the center disk can be sufficiently near the first tangency such as to not cause an error – so that this one grouping of three disks results in only one error. A fourth disk can be brought in tangent to the center disk, but still discriminate itself against the second or third disk. This one grouping still only contains one error.

There can be two tangencies to the first center disk which don’t interact, and this creates two separate groupings, each accounting for one error (see figure 7e).

In summary, note how each tangency creates a hotspot around which tangencies can cluster with only the first one counting as an error. These spots are what we are counting. E_n is a count of these groupings, as each grouping equals one error, so when we want to predict how many “good” spots there will be for the $(n + 1)$ th target to land, we know it will be approximately proportional

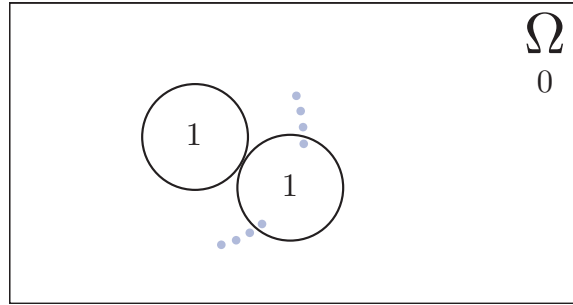


FIGURE 8. Around this cluster of targets, in our second order approximation with the left “center” disk held fixed with $h = 1$, there are on average (for the 88 possible positions of the second disk) $c = 21.455$ positions where a third disk could be centered such as to be tangent with the center disk, but not cause an error by being discriminated by the second disk. The dots represent a few of these “good points.”

to E_n . Continuing in this way,

$$\begin{aligned} E_5(\# \text{ of errors}) &\approx E_4 + \frac{4 \cdot 88_{\text{corrected}}}{A} - c \left(\frac{E_4}{A} \right) \\ &= \frac{10 \cdot 88_{\text{corrected}}}{A} - \frac{10c \cdot 88_{\text{corrected}}}{A^2} + \frac{5c^2 88_{\text{corrected}}}{A^3} - \frac{c^3 88_{\text{corrected}}}{A^4} \end{aligned}$$

Finally,

$$E_n(\# \text{ of errors}) \approx E_{n-1} + \frac{(n-1)88_{\text{corrected}}}{A} - \frac{c \cdot E_{n-1}}{A}$$

which is (7). \square

Continuing on with our proof of (6), note that (7) is a first-order linear inhomogeneous recurrence relation with variable coefficient(s), a class of recurrence relations which has an elegant solution [14], given by the following lemma.

Lemma 2.4 ([14]). *The solution to a general first-order linear inhomogeneous recurrence relation with variable coefficient(s) in the form $a_{n+1} = f_n a_n + g_n$, $f_n \neq 0$ is given by*

$$(8) \quad a_n = \left(\prod_{k=0}^{n-1} f_k \right) \left(A_0 + \sum_{m=0}^{n-1} \frac{g_m}{\prod_{k=0}^m f_k} \right)$$

Proof. Starting with $a_{n+1} = f_n a_n + g_n$, $f_n \neq 0$,

$$\begin{aligned} a_{n+1} &= f_n a_n + g_n \\ a_{n+1} - f_n a_n &= g_n \end{aligned}$$

$$\begin{aligned} \frac{a_{n+1}}{\prod_{k=0}^n f_k} - \frac{f_n a_n}{\prod_{k=0}^n f_k} &= \frac{g_n}{\prod_{k=0}^n f_k} \\ \frac{a_{n+1}}{\prod_{k=0}^n f_k} - \frac{a_n}{\prod_{k=0}^{n-1} f_k} &= \frac{g_n}{\prod_{k=0}^n f_k} \end{aligned}$$

Let

$$A_n = \frac{a_n}{\prod_{k=0}^{n-1} f_k},$$

then

$$\begin{aligned} A_{n+1} - A_n &= \frac{g_n}{\prod_{k=0}^n f_k} \\ \sum_{m=0}^{n-1} (A_{m+1} - A_m) &= A_n - A_0 = \sum_{m=0}^{n-1} \frac{g_m}{\prod_{k=0}^m f_k} \\ \frac{a_n}{\prod_{k=0}^{n-1} f_k} &= A_0 + \sum_{m=0}^{n-1} \frac{g_m}{\prod_{k=0}^m f_k} \\ a_n &= \left(\prod_{k=0}^{n-1} f_k \right) \left(A_0 + \sum_{m=0}^{n-1} \frac{g_m}{\prod_{k=0}^m f_k} \right), \end{aligned}$$

which is (8), the result we desired. \square

We are now ready to prove (6).

Proof. In (8) take $a_n = E_n = E_{n-1} \left(1 - \frac{c}{A}\right) + \frac{(n-1)88_{corrected}}{A}$, substitute $n \mapsto n+1$ in this relation to get $a_{n+1} = E_{n+1} = E_n \left(1 - \frac{c}{A}\right) + \frac{n88_{corrected}}{A}$, and then we compare this equation with $a_{n+1} = f_n a_n + g_n$, and take $f_n = \left(1 - \frac{c}{A}\right)$ and $g_n = \frac{n88}{A}$. Finally, noting that $A_0 = 0$ as $a_0 = 0$ (if no targets are put down, there are no errors), we plug what we know into (8) to get,

$$(9) \quad E_n \approx \left(1 - \frac{c}{A}\right)^n \left(\sum_{m=0}^{n-1} \frac{\frac{m88_{corrected}}{A}}{\left(1 - \frac{c}{A}\right)^{m+1}} \right)$$

$$(10) \quad = \frac{88_{corrected}}{A} \cdot \left(1 - \frac{c}{A}\right)^{n-2} \sum_{m=1}^{n-1} m \left(\frac{1}{1 - \frac{c}{A}} \right)^{m-1}$$

Which is in the form of $\sum_{k=1}^n k r^{k-1}$, a solution to which can be found by differentiating the standard geometric series formula with respect to r ,

$$(11) \quad \sum_{k=0}^n a r^k = \frac{a(1 - r^{n+1})}{1 - r}$$

$$(12) \quad \frac{d}{dr} \sum_{k=0}^n r^k = \sum_{k=1}^n k r^{k-1} = \frac{1 - r^{n+1}}{(1 - r)^2} - \frac{(n+1)r^n}{1 - r}$$

Applying (12) to (10) gives, after some algebra,

$$E_n \approx \frac{88_{corrected}}{c^2} \left(\left(1 - \frac{c}{A}\right)^n \cdot A - A + nc \right)$$

which is a relatively simple solution to our recurrence relation (7), and is the desired result (6). \square

2.6. Immediate applications. If we take the limit of $\left(n - \frac{88_{corrected}}{c^2} \left(\left(1 - \frac{c}{A}\right)^n \cdot A - A + nc \right)\right)$ as $n \rightarrow \infty$,

$$(13) \quad \lim_{n \rightarrow \infty} \left(n - \frac{88_{corrected}}{c^2} \left(\left(1 - \frac{c}{A}\right)^n \cdot A - A + nc \right) \right) = \lim_{n \rightarrow \infty} \left(n \cdot \left(1 - \frac{88_{corrected}}{c} \right) + \frac{A \cdot 88_{corrected}}{c^2} \right).$$

where $0 < c < A$, we note that $\left(n - \frac{88_{corrected}}{c^2} \left(\left(1 - \frac{c}{A}\right)^n \cdot A - A + nc \right)\right)$ diverges if $c > 88_{corrected}$ and it can become negative if $c < 88_{corrected}$. For this reason we try setting $c = 88_{corrected}$.

We then note that equation (6) with $c = 88_{corrected}$ takes into account higher order errors and holds up very well, even when we “flood the gates” so to speak by having many targets very densely packed together. Moreover, equation (6) with the this same value of c continues to hold when targets are sparsely distributed, indicating that (6) is robust (see table 2 for numerical results for large and small n).

In order to derive an improved point estimator for n , we note that for a fixed target radius and a fixed sensor field area, and with $88_{corrected} \leq c < A$, the function defined by taking n to the value given by

$$(14) \quad n - \frac{88_{corrected}}{c^2} \left(\left(1 - \frac{c}{A}\right)^n \cdot A - A + nc \right)$$

is injective.

Arguing by contradiction, we assume there are n_1 and n_2 , $n_1 \neq n_2$, and $n_1 > n_2$, such that,

$$n_1 - \frac{88_{corrected}}{c^2} \left(\left(1 - \frac{c}{A}\right)^{n_1} \cdot A - A + n_1 c \right) = n_2 - \frac{88_{corrected}}{c^2} \left(\left(1 - \frac{c}{A}\right)^{n_2} \cdot A - A + n_2 c \right)$$

then

$$\underbrace{\frac{(n_1 - n_2)}{A} \left(\frac{c^2}{88_{corrected}} - c \right)}_{\geq 0 \text{ by assumptions}} = \underbrace{\left(1 - \frac{c}{A}\right)^{n_1} - \left(1 - \frac{c}{A}\right)^{n_2}}_{< 0 \text{ by assumptions}}$$

which under our assumptions ($88_{corrected} \leq c < A$ and $n_1 > n_2$) is a contradiction. Therefore, $n_1 = n_2$ and the function which takes n to the value given in (14) is injective.

Thus, given an observed value n_{obs} of $\int_{\mathbb{R}^2} h d\chi$, we can solve

$$n_{obs} = \hat{n} - \frac{88_{corrected}}{c^2} \left(\left(1 - \frac{c}{A}\right)^{\hat{n}} \cdot A - A + \hat{n}c \right)$$

numerically for \hat{n} , and obtain a better estimate for n than simply n_{obs} . As (6) is approximately unbiased, this method of obtaining an improved estimate of n is also approximately unbiased.

Looking to expand our assumptions, an interesting case is when the sensor field is not only discretized, but the targets' centers are also continuously placed on this sensor field – a much more useful application than the discrete placement case. Imagine, for example, a discrete sensor field in front of you. You drop a pile of quarters onto it. Almost surely, not a single quarter will land with its center exactly at a point where four sensors meet; each quarter has the opportunity to drift in one direction or another. The slightest perturbation in a quarter's center coordinate away from an integer will cause it to land on sensors such as to distort its perceived shape and cause new and unforeseen errors (see figure 9). Research needs to be done into this continuous placement case.

Looking to further expand past our assumptions, the case when $r > 7$ is most interesting. With $r > 7$ disks placed discretely on a discrete sensor field, more than simple tangencies can occur. Discretized disks of larger radii can exhibit concave behavior when two identical disks join in certain precise ways to create a single element in the level sets with an Euler characteristic of zero. Larger disks can also exhibit another type of “locking behavior” where two disks join together to have an integral with respect to the Euler characteristic of 3 (see figure 10). The number of positions around a disk that another disk's center can be placed to cause these different effects varies from radius to radius, and no pattern seems to emerge (see table 1 and figure 11).

An analysis similar to that done for radii less than 8 should be applicable to greater radii.

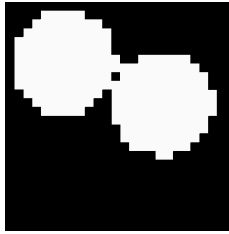


FIGURE 9. This is the level set generated from two radius = 6 disks falling onto a discrete sensor field with continuous placement of their centers. New behavior arises in this case. Here $\int_{\Omega} h d\chi = 0$, which does not occur with discrete placement.

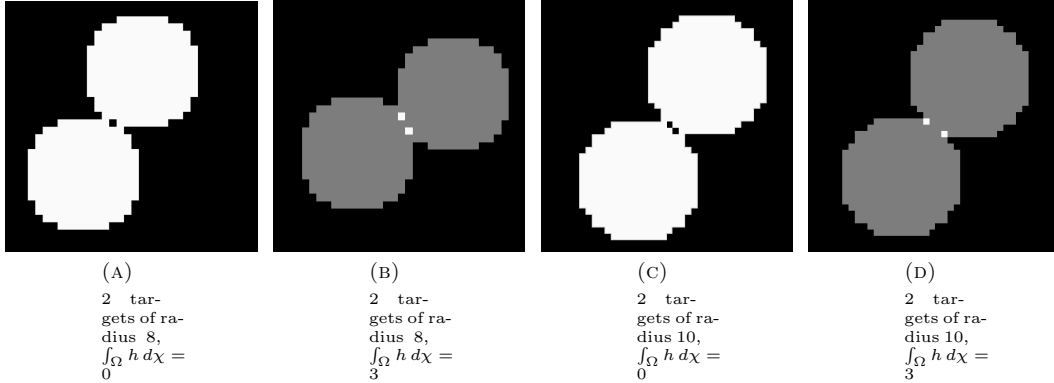


FIGURE 10. Above are examples of the ways targets of radii > 7 can join together to create different types of errors when evaluating $\int_{\Omega} h d\chi$ over a discrete sensor field.

See table 2 and figure 12 for numerical examples of our results. Observed data were generated from a virtual sensor field environment created in GNU Octave [6].

3. ASYMPTOTIC BEHAVIOR

Given an understanding of how errors in target enumeration accumulate for small n , the question then arises, how does Theorem 1.1 behave for large n ? In answering this question, a connection arises to a problem in probability called the *coupon collector's problem*. Given a set of p coupons of all different types, how many coupons does the coupon collector expect to need to draw with replacement before having at least one copy of each type of coupon? A similar question is, “How many coupons does the coupon collector expect to need to draw with replacement before having at least q copies of each type of coupon?” A solution to this more difficult multiple coupon problem is given by [16]. The link between this multiple coupon problem and Euler characteristic integrals is seen when we note that if for some integer s the $\{h = s\}$ level set covers all of Ω , then by Theorem 1.1 this level set contributes s units to the target enumeration count. If, for instance, each sensor in a sensor field picks up 10 targets, then the $\{h = 10\}$ level set will cover all of Ω , and Theorem 1.1 will return a target count of 10. In [16] it is shown that for large q , the expected number of coupons the coupon collector needs is asymptotic to pq by the law of large numbers. Thus, for a regular grid of sensors that is l sensors long and w sensors wide, and for targets that are the size of the sensors and discretely placed over the centers of sensors, this is saying that for large n , every lw targets placed over the sensor field increases by one the number of the highest level set that covers all of Ω . Then, if you put down mlw targets for some large positive integer m , you would expect the $\{h = m\}$ level set to cover Ω , which would account for mlw targets, leaving a total of $mlw - mlw = 0$ targets to fill the higher level sets. In other words, our examination shows that the highest non-empty level set of h covers Ω , and all higher level sets are empty and do not contribute to the Euler characteristic integral.

To work more generally with any setup of sensor field (assumed to be in a region Ω), and any (fixed) target shape, with targets placed uniformly and discretely, we proceed as follows. Construct a height function h' which is the return of a sensor field in which each sensor has a target centered

radius	Error Type			radius	Error Type		
	0	1	3		0	1	3
1	0	8	0	51	168	584	80
2	0	24	0	52	152	600	88
3	0	40	0	53	112	584	96
4	0	56	0	54	136	576	88
5	0	72	0	55	120	632	80
6	0	88	0	56	200	600	96
7	0	104	0	57	176	632	112
8	8	112	8	58	248	632	112
9	0	136	0	59	176	632	88
10	16	136	16	60	200	696	112
11	8	160	8	61	184	624	120
12	8	176	8	62	176	680	112
13	16	176	16	63	192	672	104
14	8	208	8	64	248	704	112
15	24	200	24	65	216	744	88
16	16	224	16	66	192	688	96
17	32	208	32	67	184	720	88
18	40	248	32	68	280	728	152
19	16	272	16	69	224	712	136
20	32	256	32	70	208	752	128
21	16	288	16	71	200	704	112
22	56	280	48	72	184	736	112
23	40	312	32	73	280	768	112
24	32	320	32	74	184	768	104
25	48	304	48	75	328	752	152
26	56	344	48	76	208	752	128
27	72	336	56	77	232	824	120
28	48	352	48	78	288	792	128
29	32	376	32	79	216	792	112
30	72	392	48	80	264	768	128
31	48	408	40	81	304	856	128
32	88	416	48	82	248	832	152
33	48	400	56	83	320	840	152
34	72	408	48	84	240	848	128
35	88	424	64	85	376	888	136
36	56	440	56	86	312	864	152
37	96	440	56	87	352	832	168
38	72	472	48	88	264	864	136
39	136	456	80	89	224	856	152
40	104	488	64	90	336	888	160
41	80	488	72	91	336	920	176
42	96	504	48	92	320	872	160
43	56	536	56	93	304	944	120
44	144	512	80	94	376	952	152
45	104	544	64	95	368	912	184
46	152	496	88	96	352	960	152
47	152	552	88	97	344	904	168
48	96	536	80	98	400	1008	128
49	136	520	104	99	448	912	200
50	112	632	72	100	408	952	184

TABLE 1. For varying radius and discrete placement with integer centers, the above table gives the number of positions around a discrete disk where, when another identical disk is placed there, $\int_{\mathbb{R}^2} h d\chi = 0, 1$, or 3 (which we call type 0, 1, or 3 errors).

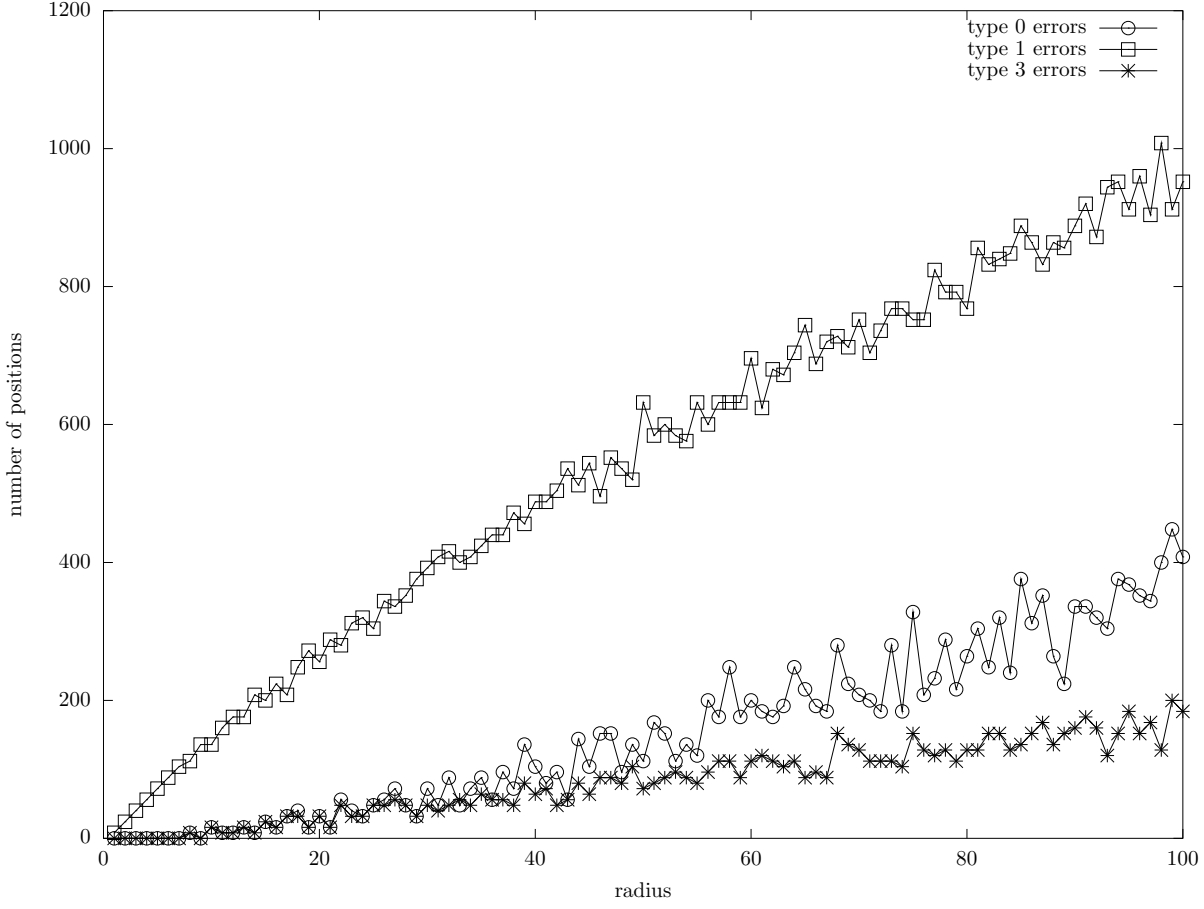


FIGURE 11. A plot of table 1.

over it. Let,

$$(15) \quad H = \int_{\Omega} h' d\chi$$

Let α be the number of sensors in our sensor field. Then when n targets are uniformly and discretely put down, where $n = m \cdot \alpha$ for some positive integer m , and where h is the height function coming off this sensor field, by (1), (15) and the above reasoning, we have

Theorem 3.1.

$$(16) \quad \int_{\Omega} h d\chi = Hm, \quad \text{as } n \rightarrow \infty$$

n	observed	Formula (5), $b = 88_{corrected}$	Formula (6), $c = 21.455$	Formula (6), $c = 88_{corrected}$
100	98.294	96.5	98.2	98.2
200	193.12	185.7	192.9	193
300	284.72	267.9	284.1	284.5
400	373	342.8	371.7	372.7
500	458.5	410.6	456	457.8
600	541.04	471.2	536.8	540
700	619.55	524.7	614.2	619.2
800	697.11	571.0	688.2	695.7
900	771.23	610.1	758.9	769.4
1 000	843.67	642.1	826.3	840.6
2 000	1 446.2	567.6	1 324.9	1 428
3 000	1 881.5	-223.4	1 524.1	1 838.5
4 000	2 178.9	-1 731.0	1 449.7	2 125.4
5 000	2 390.0	-3 955.2	1 125.2	2 325.9
6 000	2 524.1	-6 895.9	572.1	2 466
7 000	2 611.1	-10 553.2	-189.7	2 563.9
8 000	2 663.2	-14 927	-1 142.4	2 632.4
9 000	2 689.8	-20 017.4	-2 269.4	2 680.2
10 000	2 703.2	-25 824.3	-3 555.9	2 713.6

TABLE 2. For a 500×500 discrete sensor field with n radius = 6 targets put down uniformly and discretely, the observed value (averaged over 1 000 trials) of $\int_{\mathbb{R}^2} h d\chi$ is presented, along with $E(\int_{\mathbb{R}^2} h d\chi)$ calculated using (5) and then the second-order (6) with both the second-order value of c and with $c = 88_{corrected}$. For this region, $88_{corrected} = 85.322$.

4. CONCLUSION

The main result in this paper is (6), which gives an approximation to the bias of the Euler characteristic integral as a point estimator for n , the number of targets over a discrete sensor field. Numerical results show that equation (6) agrees closely with observations.

But this is just a preliminary analysis, and there is still much to be done. There are also many constraining assumptions we made here which are ripe for relaxing. Areas of further research might include looking into,

- The discrete Euler integral's complete probability distribution, or even just its variance.
- A generalization of the numerical analysis theory to any distribution of targets.
- A generalization to any target shape (and not just 2-d projections of discrete disks!).
- Generalizations to multiple target shapes on the same field.
- Non-regular sensor grids.
- The error tolerance and stability of the discrete integral in the face of noisy data, broken sensors, or other real world problems. Future work should include a numerical analysis of the theoretical work done on the Euler characteristic integrals of Gaussian random fields [3], which permits, at least theoretically, unbiased target enumeration off noisy sensor fields.

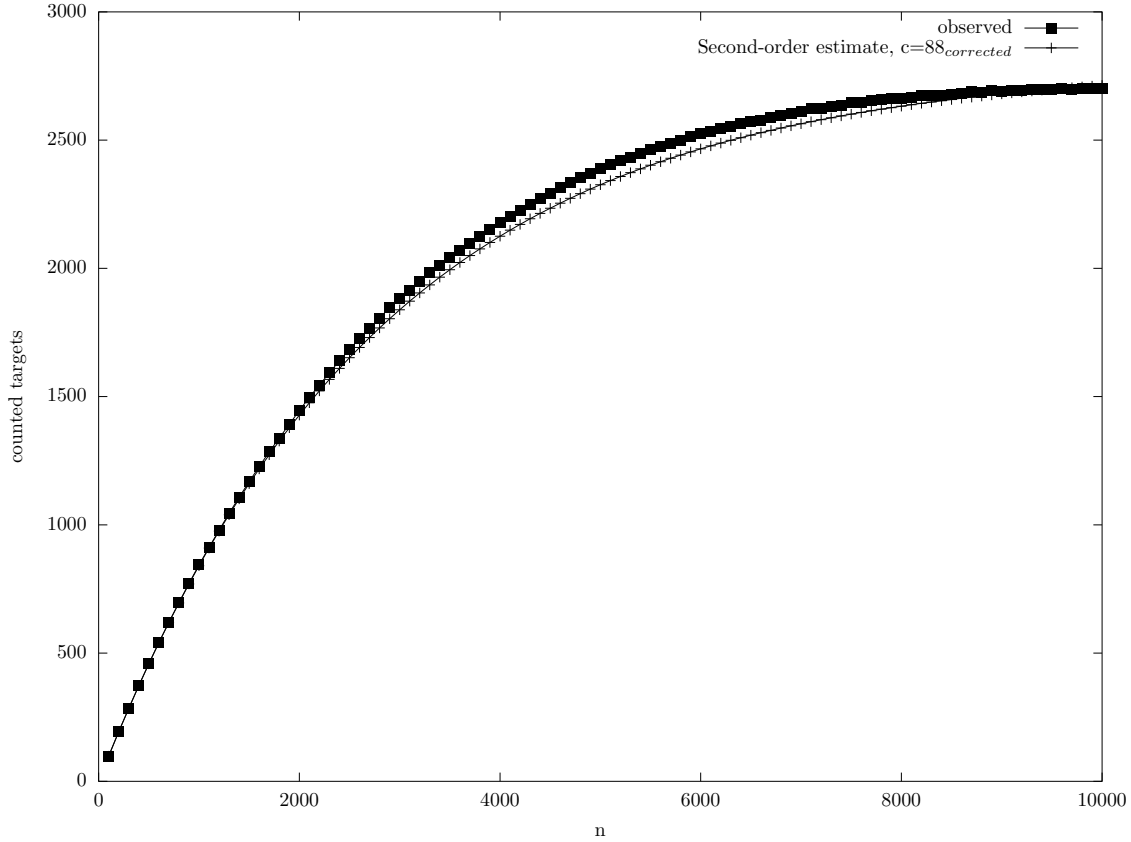


FIGURE 12. A plot of table 2: observed values of the Euler integral alongside our second-order estimates.

- The techniques for discrete Euler integral analysis and signal processing suggested in [2] and [1].
- Improving our target enumeration estimate by analysis of time series data for moving targets, similar to [18].
- Extending the work done here to targets that are continuously placed onto a sensor field, as opposed to discretely placed with integer center coordinates.

Possible applications of any numerical analysis will require additional work. All theory discussed in this article has been based on a priori knowledge of target shape and target distribution. This suggests possible areas of research into relaxing of these requirements in some way. We should try to determine estimates for these parameters from the data we are given – a sensor field.

REFERENCES

- [1] Y. Baryshnikov and R. Ghrist. Target enumeration via euler characteristic integrals. *SIAM Journal on Applied Mathematics*, 70(3):825–844, 2009.

- [2] Y. Baryshnikov and R. Ghrist. Euler integration over definable functions. *Proceedings of the National Academy of Sciences*, 107(21):9525–9530, 2010.
- [3] O. Bobrowski and M. Strom Borman. Euler Integration of Gaussian Random Fields and Persistent Homology [arXiv:1003.5175v3 \[math.PR\]](#).
- [4] A. Boulis, S. Ganeriwal, and M. Srivastava. Aggregation in sensor networks: an energy-accuracy trade-off. *J. Ad-hoc Networks*, 1:317–331, 2003.
- [5] Justin Curry, Robert Ghrist, and Michael Robinson. Euler calculus with applications to signals and sensing. *Proceedings of Symposia in Applied Mathematics*. To appear.
- [6] John W. Eaton. *GNU Octave Manual*. Network Theory Limited, 2002.
- [7] D. Estrin, D. Culler, K. Pister, and G. Sukhatme. Connecting the physical world with pervasive networks. *IEEE Pervasive Computing*, 1:59–69, 2002.
- [8] Qing Fang, Feng Zhao, and Leonidas Guibas. Lightweight sensing and communication protocols for target enumeration and aggregation. In *Proceedings of the 4th ACM International Symposium on Mobile ad hoc Networking & Computing*, pages 165–176. ACM Press, 2003.
- [9] L. Guibas. Sensing, tracking and reasoning with relations. *IEEE Signal Processing Mag.*, 19, 2002.
- [10] Allen Hatcher. *Algebraic Topology*. Cambridge University Press, 1 edition, December 2001.
- [11] T. He, P. Vicaire, T. Yan, L. Luo, L. Gu, G. Zhou, R. Stoleru, Q. Cao, J. Stankovic, and T. Abdelzaher. Achieving real-time target tracking using wireless sensor networks. In *Proceedings of IEEE Real Time Technology and Applications Symposium*, pages 37–48, 2006.
- [12] B. Jung and G. Sukhatme. A region-based approach for cooperative multi-target tracking in a structured environment. In *Proceedings of IEEE/RSJ Conference on Intelligent Robots and Systems*, 2002.
- [13] Zenon Kulpa. On the properties of discrete circles, rings, and disks. *Computer Graphics and Image Processing*, 10:348–365, 1979.
- [14] Dr. Keh-Yi Lee. Chapter 15 difference equations and the z-transforms. <http://faculty.pccu.edu.tw/%7Emeng/Math15.pdf>.
- [15] D. Li, K. Wong, Y. Hu, and A. Sayeed. Detection, classification, and tracking of targets. *IEEE Signal Processing Mag.*, 19:17–30, 2002.
- [16] Donald J. Newman and Lawrence Shepp. The double dixie cup problem. *The American Mathematical Monthly*, 67(1):58–61, 1960.
- [17] Sheldon Ross. *A First Course in Probability*. Prentice Hall, 8 edition, January 2009.
- [18] J. Singh, U. Madhow, R. Kumar, S. Suri, and R. Cagley. Tracking multiple targets using binary proximity sensors. In *Proceedings of the 6th International Conference on Information Processing in Sensor Networks*, pages 529–538, 2007.
- [19] J. Zhao, R. Govindan, and D. Estrin. Computing aggregates for monitoring wireless sensor networks. In *Proceedings of IEEE Intl. Workshop on Sensor Network Protocols and Applications (SNPA)*, 2003.

UNIVERSITY OF PENNSYLVANIA, 3650 CHESTNUT STREET, PHILADELPHIA, PA, USA

E-mail address: krupa@sas.upenn.edu